LA-UR- 09-03019

Approved for public release; distribution is unlimited.

Title:	Thermal Analysis of Pentaerythritol Tetranitrate and Development of a Powder Aging Model
Author(s):	Geoffrey W. Brown (DE-1) Mary M. Sandstrom (DE-1) Anna M. Giambra (DE-1) Jose G. Archuleta (DE-1) Deirdre C. Monroe (W-6)
Intended for:	37th Annual Conference of the North American Thermal Analysis Society, Lubbock, TX, Sept 20-23, 2009

Los Alamos
NATIONAL LABORATORY
EST. 1943

Form 836 (7/06)

Thermal Analysis of Pentraerythritol Tetranitrate and Development of a Powder Aging Model

Geoffrey W. Brown[1], Mary M. Sandstrom[1], Anna M. Giambra[1], Jose G. Archuleta[1], and Deirdre C. Monroe[2]
[1]High Explosive Science & Technology (DE-1), MS C920
[2]Detonator Technology (W-6), MS P950
Los Alamos National Laboratory, Los Alamos, NM 87545
Contact e-mail: geoffb@lanl.gov

ABSTRACT

We have applied a range of different physical and thermal analysis techniques to characterize the thermal evolution of the specific surface area of pentaerythritol tetranitrate (PETN) powders. Using atomic force microscopy we have determined that the mass transfer mechanism leading to powder coarsening is probably sublimation and redeposition of PETN. Using thermogravimetric analysis we have measured vapor pressures of PETN powders whose aging will be simulated in future work. For one specific powder we have constructed an empirical model of the coarsening that is fit to specific surface area measurements at 60 °C to 70 °C to provide predictive capability of that powder's aging. Modulated differential scanning calorimetry and mass spectroscopy measurements highlight some of the thermal behavior of the powders and suggest that homologue-based eutectics and impurities are localized in the powder particles.

INTRODUCTION

Pentaerythritol Tetranitrate (PETN, $C(CH_2OH)_4$) is an explosive material that is used in powder form in detonators because of its initiation properties and power. PETN detonation properties are strongly influenced by the particle size distribution of the powder, with the average particle size of the powder often characterizing the batch. The dependence of detonation properties on this distribution is an issue for aging and storage of explosive devices since PETN coarsens due to thermal energy input from the environment [1]. This coarsening is a well known problem although the actual mechanism is not well understood. It is important to understand PETN aging so that predictive models can be constructed that will benefit projects addressing with the storage and lifetime of explosive devices. In this work we are concerned with behavior of the powders at temperatures from 30 °C to 80 °C over extended periods of time.

PETN particle coarsening necessarily occurs via mass redistribution from smaller particles to larger particles. (Previous unpublished results do show small changes in individual particle shapes due to aging [2], but these changes are not large enough to account for the observed coarsening.) Two possible redistribution mechanisms are vapor phase material transfer through a sublimation-redeposition process and solid-state mass transfer through surface mass diffusion between connected particles. Both processes are thermally driven and will involve detachment of mass from relatively stable points on the particle surfaces. As such, thermal analysis and other particle characterization techniques can provide insight into the mechanism of, and detailed characteristics of, the coarsening. Decomposition is not expected to play a role in low temperature studies of the powders since it would cause particle sizes to drop as mass is lost to volatile gas phase species. At higher temperatures, beyond the range we examine in this paper, decomposition does become important, especially in enclosed containers since the process is autocatalytic and dependent on NO_2 concentrations [3].

When considering sublimation-driven processes as possible coarsening mechanisms, the vapor pressure of the material becomes an important physical parameter. The vapor pressure is a function not only of the intrinsic crystal bonding, but also of impurity content, extrinsic stabilization mechanisms, particle size, etc. It is important then to measure the vapor pressure of specific powders of interest to be able to make predictions about their behavior. Several measurements of PETN vapor pressure are available in previous publications [4,5] but they cannot immediately be adapted for our powders because of the the factors just noted and since the studies did not report details of the powders for which the measurements were made.

In this work we have examined PETN powders using a variety of experimental methods to try to understand aging. We have used permeametry to study the evolution of average particle size in bulk powders as a function of temperature – this is the basic coarsening process. We have used atomic force microscopy (AFM) to observe thermally driven changes in individual particles. The AFM data suggest a coarsening mechanism that leads to an empirical, physically-motivated coarsening model that is fit to permeametry data. To provide input to simulations based on that model and verify its consistency, we have used optical microscopy-based particle size analysis to characterize particle size distributions. Finally we have used modulated differential scanning calorimetry (mDSC), thermogravimetric analysis (TGA), and mass spectroscopy (MS), to characterize the thermal properties of the materials, including their vapor pressures. These data will provide input to improved powder coarsening simulations in the near future.

BACKGROUND

PETN is made by nitrating pentaerythritol with HNO_3. Particle size distributions can be adjusted by recrystallizing the PETN to obtain the desired average particle size for a particular detonation application. Recrystallization is typically carried out by dissolving the coarse powder in acetone and then crash precipitating it back out of solution by adding water, which also serves as a purification step. Remaining solvent and water are driven off with heat. Recrystallization process parameters such as the rate of water addition are used to adjust the particle size distributions. Mean surface areas of the final dry powder, as measured by our permeametry instrument, can range from below 3000 cm^2/g to greater than 20,000 cm^2/g, corresponding to average particle sizes of > 11 microns to < 2 microns, respectively. The distributions are typically broad, ranging from submicron size particles to particles with long dimensions > 20 microns, presumably because of the stochastic nature of the nucleation process that begins the precipitation.

The powder particles from the precipitation process are relatively crystalline. At room temperature (and over the range of temperatures examined here) PETN has a $\underline{P}42_1\underline{c}$ crystal structure with lattice constants of $a = b = 9.38$ Å and $c = 6.71$ Å. The equilibrium shape of a PETN crystal is slightly rectangular with an aspect ratio near 1, however, because of the relatively rapid nature of the precipitation process, particles observed in powders are elongated with aspect ratios exceeding 5 in many cases. The PETN system is complicated by the existence of homologues that arise in the manufacturing process. These homologues can generally be described as combinations of 2 or 3 PETN molecules. The homologues complicate the thermal behavior of the system by forming eutectic compositions with PETN itself. The phase diagram of the homologoue system has been mapped previously [6].

EXPERIMENTAL

We characterized the particle size and specific surface area of the PETN powders using a Model 95 Fisher Scientific Sub-sieve Size Analyzer (FSSSA). The FSSSA measures an average particle diameter through the equilibrium pressure drop that occurs as gas permeates a packed

powder. In our work we convert this diameter to specific surface area using formulas provided in the operation manual [7]. The conversion from pressure drop to particle size and the formula for calculating the corresponding specific surface area are both based on fluid dynamics analysis of the method and instrument.

AFM images of PETN particles were acquired with a Veeco Instruments CP-II atomic force microscope. Images were acquired in non-contact mode with silicon cantilevers having a ~300 kHz resonance. The imaging tips on the ends of the cantilevers have ~10 nm radius of curvature. During each raster scan we typically map the topography of the surface, the error signal of the scanner, and the phase difference between the cantilever's oscillation drive and response signals. Powder samples were prepared by placing < 10 mg of PETN onto acrylate-based double sided tape attached to an AFM sample disk. Loose PETN was then gently tapped off of this sample mount.

We analyzed the particle size distribution (PSD) of the starting PETN using a Malvern Pharmavision 830, which is an automated optical microscope with particle counting software. PETN was dispersed in heptane and samples were prepared by allowing a drop of the PETN/heptane mixture to evaporate on a glass slide. Remaining agglomerates were removed from the PSD analysis using an operator-assigned maximum single particle size. The minimum measurable particle size using this instrument is stated to be 0.7 microns although in our experience with PETN dispersions, particles below 1 micron are not accurately counted.

For PETN aging, ~ 6 g powder samples were hermetically sealed in polymer-coated aluminum containers and heated in a laboratory oven. Multiple identical cans were aged simultaneously and replicates were pulled at different times for FSSSA measurement to characterize the specific surface area evolution. In this work we report results for PETN aged at 60 °C and at 70 °C for ~ 600 and ~ 800 hours, respectively.

Vapor pressures were measured using isothermal TGA with a TA Instruments Q5000. The analysis technique is described in other publications [8]. The mass loss of benzoic acid was used to determine the constants relating vapor pressure to mass loss for the instrument, temperature range, sample pans, and gas flow rate, used in our experiments. These constants were then applied to the PETN mass loss data for samples run under identical conditions to determine the PETN vapor pressure as a function of temperature.

Modulated DSC measurements were made using a TA Instruments Q1000. The temperature was ramped from 50 °C to 100 °C at 0.2 °C/min with a thermal modulation of 0.133 °C every 60 seconds (or every 0.2 °C). The samples were 8 to 10 mg in mass and they were lightly pressed onto the bottom of an aluminum sample pan. The pan was covered with a crimped lid, but the lid was not hermetically sealed to the pan, allowing volatile gases to escape and avoiding autocatalytic activity.

Mass spectroscopy of evolved species was measured with an Netzsch Instruments Aëolos QMS 403 C while the sample was heated at 0.2 °C/min in a Netzsch Instruments STA409 DSC/TGA. UHP argon was the carrier gas and the gases evolved from the sample were transferred to the QMS through a glass capillary tube held at 80 °C. The heated tube did cause decomposition of some evolution products and so, for this analysis, total ion current as a function of time was monitored as a function of temperature.

We examined 8 different PETN powders in this work. All powders were made with slightly different parameters or from different starting materials. For the aging model development we concentrate on a single powder, denoted PETN 1. Results for all 8 powders are presented for a subset of the analytical methods just described.

RESULTS

Figure 1 shows AFM error signal images of typical PETN particles in our powders. The left image covers a 10 micron by 10 micron area and the right image covers a 5 micron by 5 micron area. The rough region around the particles is the surface of the mounting tape. In each case we observe large and small particles, demonstrating the range of sizes that exist in the powders. The large particles are elongated due to the non-equlibrium precipitation process and have relatively rough edges and other surface asperities that slightly increase their surface area. Steps are visible on the surfaces of all particles and are generally parallel to the long or short axes of the particle, although there are transition regions visible.

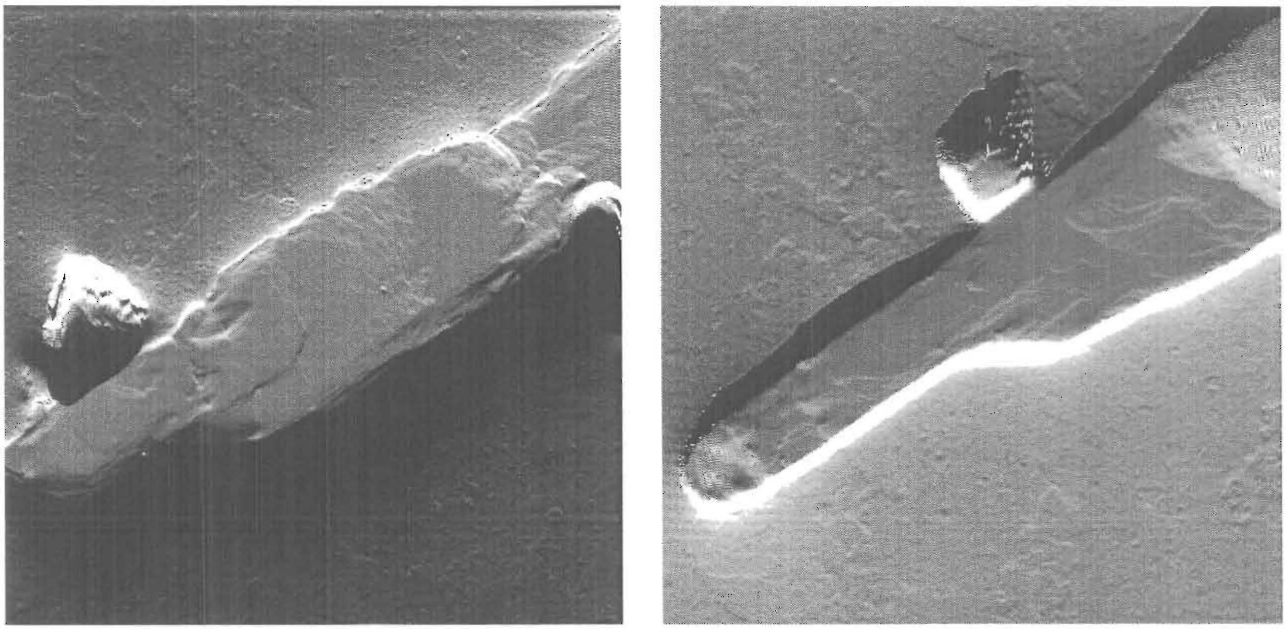

Figure 1. Left panel: 10 micron x 10 micron error signal AFM image of PETN particles. Right panel: 5 micron x 5 micron error signal AFM image of different PETN particles.

Figure 2 shows a close up of steps on two other particles and a section through the AFM data in the middle image. The left panel is a 1.5 micron by 1.5 micron phase image. Phase images tend to be more sensitive to the small vertical changes at terrace edges. In that image it is also possible to discern very fine step structure on the steeply sloped sides of the particles, illustrating their crystalline nature. The middle image is a topographic scan covering a 200 nm x 200 nm area of a different particle. The wavy nature of some of the step edges is likely due to instrumental noise. A section through the leftmost step of the middle image is shown in the right panel. The measured step height is between 7 and 10 Angstroms, consistent with the lattice constants noted above. The top terrace defining the step is therefore likely a single molecular layer of PETN. The layer normal is probably perpendicular to the *c* direction, based on the shape of the particles observed, but the noise in the topography data does not let us make an unambiguous assignment. Section plots taken from other particles are often taller than 10 Angstroms and are likely multiples of molecular crystal layers.

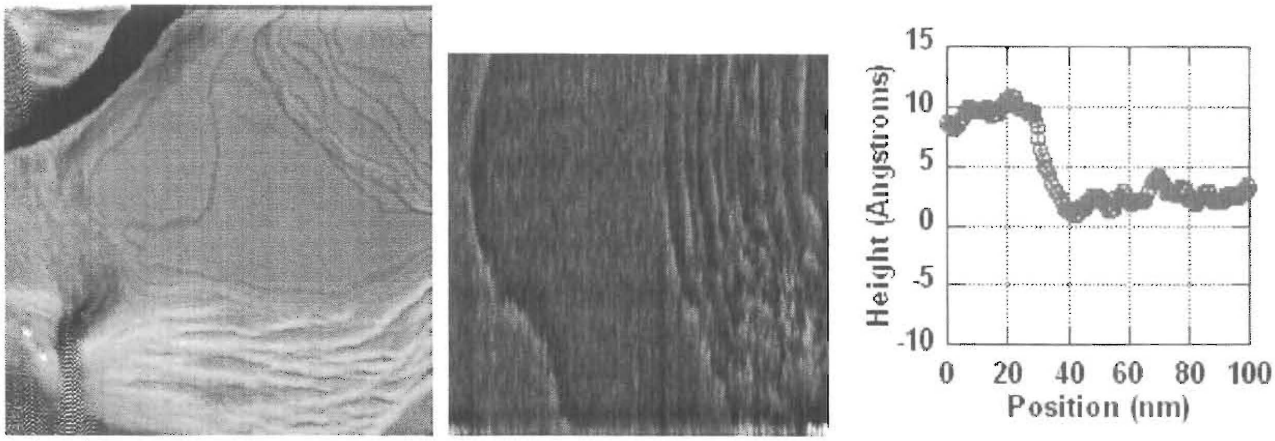

Figure 2. Left panel: 1.5 micron x 1.5 micron AFM phase image of the surface of a PETN particle. Middle panel: 200 nm x 200 nm topographic AFM image of steps on a different PETN particle. Right panel: Section plot through the topographic data in the middle panel showing the height of the leftmost step.

The steps on the surfaces of all of the particles we observe are mobile at room temperature. Steps always move towards the centers of particles and examination of the topographic images shows that the steps always move towards higher terraces, indicating that mass is moving from the step edges toward the particle boundaries. By varying the time between image acquisitions, we have verified that the step motion is not induced by the AFM tip. Step speeds at room temperature are typically ~1 nm/min.

The AFM images in figure 3 show long term particle evolution. The tape background has been digitally removed for clarity. The particle loses considerable mass over 460 minutes that elapse between the panels. The AFM images do not show how the mass is lost. Two possible mechanisms are sublimation or dissolution into the tape. It is likely that both processes are active. Dissolution must be occurring since the rate of mass loss is too high, relative to other studies of sublimation. In addition it is known that small nitrates readily dissolve into acrylate-based adhesives like the mounting tape we use to hold the powders. (This dissolution is the basis of transdermal patch basesd pharmaceuticals. The suggestion then is that the mounting tape is acting as a second mass sink for the PETN particle. Molecules thermally detach from step edges and are removed from the particle by sublimation or by dissolution when they reach the tape.

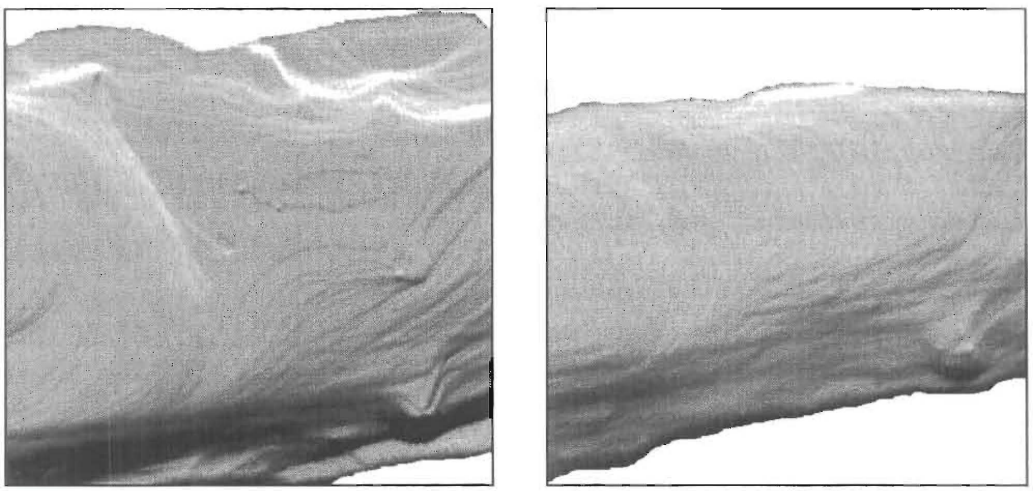

Figure 3. AFM phase images of a single particle at time zero (left) and after 460 minutes at room temperature (right). Image areas are 1.5 micron x 1.5 micron. The tape surface has been digitally removed for clarity.

Redistribution of PETN must occur due to sublimation and surface mass diffusion since each is thermally activated. Sublimation can occur directly from step edges or from open terraces after detachment. Surface mass diffusion would also occur along step edges or across open terraces after detachment. We argue that our AFM images favor sublimation for mass redistribution because PETN reattachment to step edges is not observed. Steps continually move in one direction and particles continually shrink. If surface mass diffusion were to play a significant role in mass redistribution, we should see it occurring either as temporary growth of islands like the one shown in Fig X or through slower mass loss in the regions between two islands or between an island and set of terraces. Neither of these effects is observed and our images indicate that PETN remains mobile until it is lost from the particle. This favors a sublimation-redeposition mechanism for coarsening.

Since the AFM data contain both sublimation and dissolution effects, we used isothermal TGA to determine the vapor pressures of the bulk PETN powders. Figure 4 shows an example of weight loss vs. time curves for one powder in the left panel. The right panel shows vapor pressure vs. temperature data calculated from the full set of weight loss data for all powders.

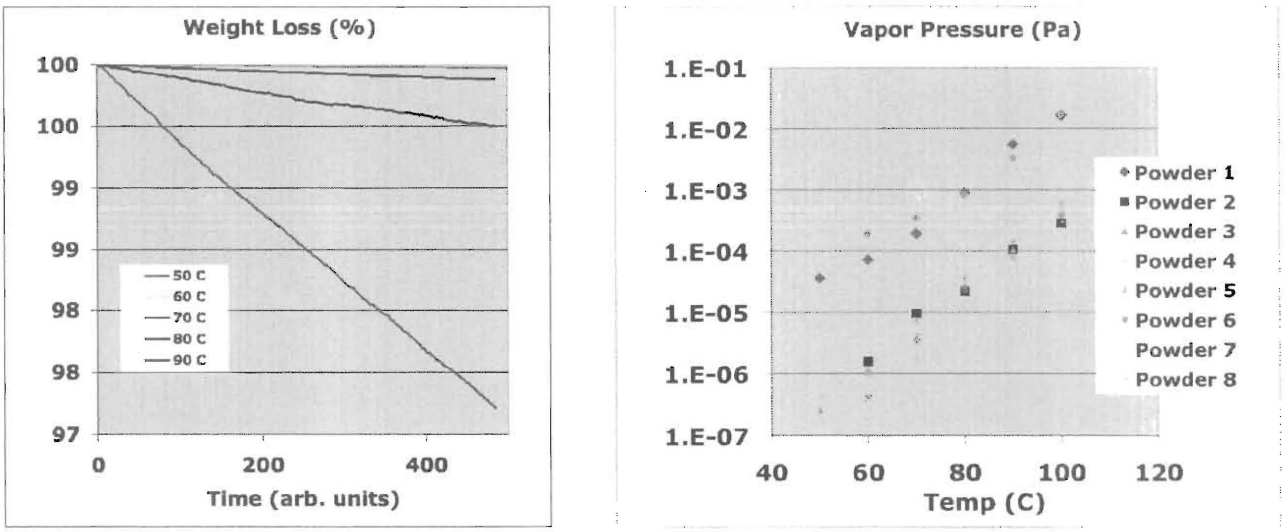

Figure 4. Left panel: Example of mass loss vs. time signals used to determine vapor pressure for one of the PETN powders examined in this work. Right panel: Vapor pressures of 8 different PETN powders calculated from data sets such as the one shown in the left panel.

As shown in Fig 4, the vapor pressure of PETN for most powders at room temperature is in the 10-8 Pa range, consistent with some of the published values. Some of the powders however do show much higher vapor pressures, by up to a factor of 100. Work is currently underway to determine the physical and chemical properties responsible for this high vapor pressure. We can say at this point that it is not due solely to particle size distribution or starting materials.

Examples of the modulated DSC data are shown in figure 5. In these cases we see three endothermic features in the non-reversible heat flow signal. The fact that they appear primarily in the non-reversing heat flow signal indicates that they are likely associated with kinetic processes such as sublimation or decomposition. The differing locations of the features from powder to

powder indicate different processes or materials are responsible. In some powders, up to five endotherms were observed.

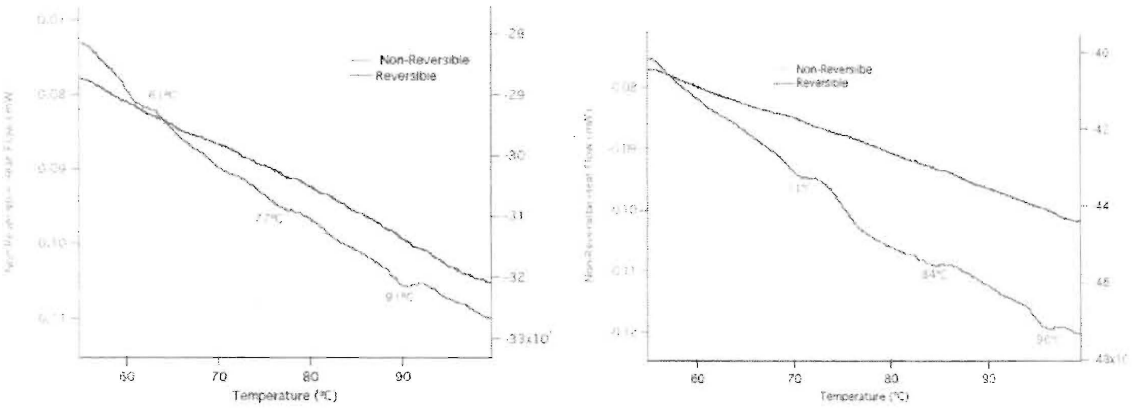

Figure 5. Modulated DSC examples from two powders.

The mass spectroscopy measurements did not show constant gas evolution for any of the powders up to 100 °C at the 0.2 °C/min ramp rate used. Instead there were specific temperatures at which the total ion current spiked for approximately 10 minutes and then dropped to zero. A table showing the corresponding temperatures of these spikes and the locations of the mDSC endotherms is shown below. There is a good correlation between the peak signal temperatures and the endothermic mDSC features.

Table 1: Table of mDSC endotherm temperatures and peak mass spectroscopy signals for the various powders.

Powder	Endotherm Temp (C)	Mass Spec Peak Signal Temp (C)
PETN 1	61 77 91	-- 74 --
PETN 2	64 75 85	63 72-76 81-84
PETN 3	63 76 93 97	65 77 92-93 97-98
PETN 4	62 68 71 81 87	-- 66 72 81-83 87
PETN 5	68 83 94	-- -- 100
	71	76

PETN 6	84 96	-- 94

Our interpretation of the QMS and mDSC observations is that they primarily correspond to volatilization of melted homologues or eutectic mixes. Many do correspond to melt ranges observed in other work [6]. We don't expect that we have seen the melt since this would occur in the reversing signal but instead we see the volatilization of the liquid phases, Also the peaked nature of the signals indicates localization of pockets of the eutectics.

These thermal analysis results are then suggesting that the PETN is not dominated by homologue material interactions. They are visible but do not greatly influence the sublimation over long periods of time. Instead, the differences we observe in vapor pressure and thermal stability are likely due to particle size distributions and perhaps other impurities that do not directly react with PETN over the temperature range we are examining.

Given the above observations, for purposes of modeling the aging behavior of the powders, we treat each PETN as a simple homogeneous material with slightly different vapor pressures. For the rest of the results and analysis described below, we concentrate on a single powder, PETN 1, in order to demonstrate the development of the aging model.

Figure 6 shows the specific surface area evolution of our PETN at 60 °C and 70 °C. Each plot symbol is the average of three replicate measurements from a single aging container. The behavior is typical of PETN. There is an initial approximately linear drop in specific surface area followed by a slower tail extending to longer times. Analysis of the tail region shows that it follows a power law dependence on time with an exponent of 0.7. Long term power law behavior is well understood from Ostwald ripening theory [9] and represents narrowing of the PSD towards its mean.

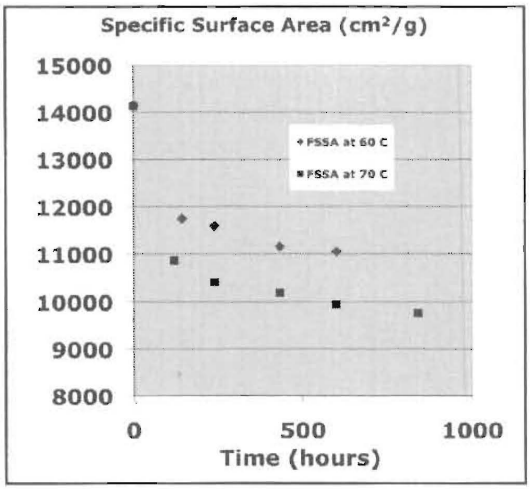

Figure 6. Plot of the evolution of specific surface area vs. time at two different temperatures for PETN powder 1.

The Pharmavision PSD for this PETN is shown in Figure 7. Values below 1 micron are not representative because of limitations of the optical method. We have verified this with AFM images and SEM images that show many particles in the powder with diameters below 1 micron. In addition, converting the distribution in Fig. 7 to a specific surface area yields a much lower value than the zero time value in the plot in Fig. 6.

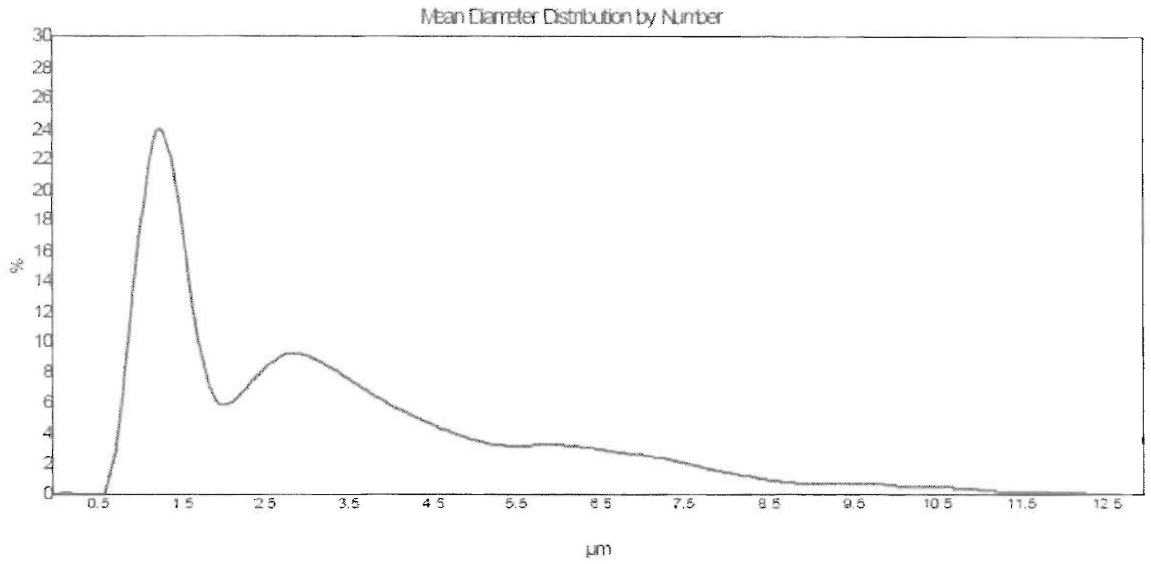

Figure 7. Plot of particle size distribution for PETN powder 1 determined by optical microscopy.

Based on these arguments, we carried out simulations of sublimation-redeposition. We treated all particles as spheres and produced a starting set of particle diameters that was qualitatively similar to the PSD in Figure 7. We then added distributions of particles peaked at 0.25 micron and 0.5 micron diameter to bring the overall specific surface area of our model powder closer to the starting value in Figure 6. The algorithm we iterated on this PSD consisted of 1) a sublimation step to remove mass from each particle, 2) a corresponding increase in PETN background pressure, 3) a redeposition step based on kinetic theory with this background pressure as input, and 4) a subsequent decrease in the PETN background pressure. The time steps of the iteration were chosen so that the 0.25 micron particles lasted for at least ~ 100 iterations at 70 °C.

Loss of mass from each particle during the sublimation step is governed by a vapor pressure, or equivalently by an activation energy and attempt frequency. For a distribution with very small particles, the sublimation must take into account the Kelvin effect [10] in which the radius of curvature influences the sublimation rate. In a simple picture, a particle with a smaller diameter (higher curvature) has a higher step density which can lead to faster sublimation since particles at step edges are less tightly bound. The equation governing the sublimation process and mass loss per unit area in each step can then be written

$$\Delta m_{-} = p_{\infty}(T)\exp\left(\frac{C}{Tr}\right)\sqrt{\frac{M}{2\pi RT}}\Delta t \qquad (1)$$

Where $p_{\infty}(T)$ is the vapor pressure of very large PETN particles, C is a constant that includes the radius of curvature of the particle, M is the molecular mass, and R is the gas constant.

Redeposition from the gas phase is based on kinetic theory. Since the incident collision rate and sticking coefficient would be the same for all particle sizes, there is no dependence on particle diameter. The mass gain for each particle can be written

$$\Delta m_+ = p\sqrt{\frac{M}{2\pi RT}}\Delta t \qquad (2)$$

Where p is the background PETN partial pressure.

As noted above, we do not know the vapor pressure of our powder nor do we have a quantitative measure of the PSD below 1 micron, but we can examine qualitative evolution. Iterating these equations to simulate mass loss in our model particle distribution leads the behavior shown in the left panel of Figure 8. At 60 °C and 70 °C we reproduce the initial linear region and slow tail at longer times. The slight downturn in the 70 °C plot is an artifact of limitations on the number of particles used in the simulation. The behavior qualitatively reproduces the observed evolution including the long term power law behavior.

Since this suggests that we understand the primary mechanism, we construct an empirical model of the coarsening from a piecewise function that includes a linear initial part (since sublimation from the smallest particles dominates at early times) and an Ostwald ripening-based power law tail. Schematically this is

$$\begin{aligned} FSSA &= At \quad \text{for } t < t' \\ &= Bt^D \quad \text{for } t > t' \end{aligned} \qquad (3)$$

Where A, B, D, and the crossover point t' are all fit to the experimental data at 60 °C and 70 °C. The results are shown in the right panel of Figure 8. This will be used to determine how the coefficients change with temperature so that predictions below 60 °C can be made.

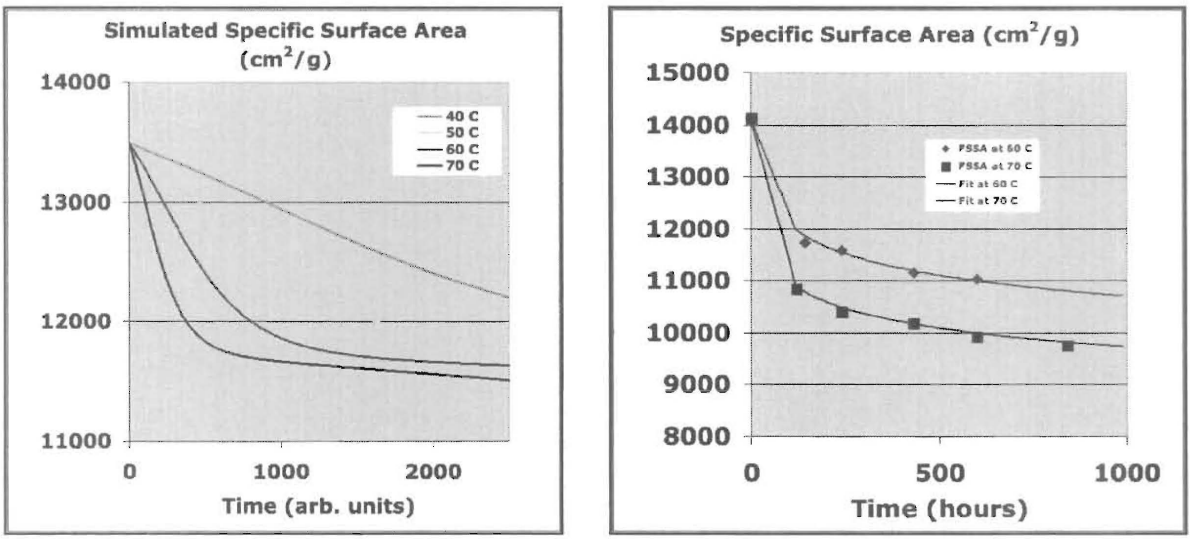

Figure 8. (left) Simulation results using the algorithm and equations listed in the text. Curves from top to bottom are for 40 °C, 50 °C, 60 °C, and 70 °C, respectively. (right) The result of fitting the data in Figure 1 with Eq. 3 at 60 °C (blue diamonds) and 70 °C (black squares).

At the time of the development of this model, we did not have the vapor pressure measurements described above. Now that those are available, we will go back and reformulate a model that uses different and fewer fit parameters to improve the physical basis of the aging predictions.

REFERENCES

[1] A. Duncan, Mason & Hanger-Silas Mason Co Report no. MHSMP-72-21, **1972**.
[2] E.L. Roemer and D.C. Monroe, Unpublished.
[3] C.M. Tarver, T.D. Tran, and R.E. Whipple, Prop. Exp. And Pyro. **2003**, *28*, 189.
[4] G. Edwards, Trans. Faraday. Soc., **1953**, *49*, 152.
[5] K.H. Lau et. al., J. Chem. Eng. Data **2004**, *49*, 544.
[6] H.H. Cady, LASL Report LA-4486-MS, **1972**.
[7] "Fisher Model 95 Sub-Sieve Sizer Manual", Catalog 14-311, Fisher Scientific Co., Pittsburgh, PA.
[8] Elder J.P., J. Therm. Analysis, **1997**, *49*, 897.
[9] L. Shi and D.O. Northwood, Phys. Stat. Sol. (a), **1992**, *133*, K1.
[10] S.W. Thomson, Phil. Mag., **1871**, *4*, 448.

ACKNOWLEDGEMENTS

This work was carried out for the United States Department of Energy at Los Alamos National Laboratory under Contract No. DE-AC52-06NA25396. The work was funded by the LANL Enhanced Surveillance Campaign.